Available online at www.sciencedirect.com
ScienceDirect
Journal of the European Ceramic Society 30 (2010) 2937–2946
www.elsevier.com/locate/jeurceramsoc

Spark plasma sintering: A powerful tool to develop new silicon nitride-based materials

M. Belmonte *, J. González-Julián, P. Miranzo, M.I. Osendi

Institute of Ceramics and Glass (CSIC), Kelsen, 5, 28049 Madrid, Spain

Available online 6 February 2010

Abstract

Several key topics on the current assisted sintering of Si_3N_4-based materials are reviewed. First, different proposed mechanisms for spark plasma sintered (SPSed) ceramics are presented, discussing the electric field effect on the liquid phase behaviour and how it may influence the liquid phase sintering of Si_3N_4 ceramics. Next, we show that the SPS is a powerful tool to develop new Si_3N_4-based materials with tailored microstructures, such as functionally graded materials (FGMs) and carbon nanotubes (CNTs) containing Si_3N_4 matrix composites. Si_3N_4 FGMs are fabricated from a sole homogenous Si_3N_4 mixture just modifying the SPS system punches set-up, thus creating a temperature gradient through the specimen. Finally, the capability of SPS to get dense Si_3N_4/CNTs composites overcoming both constraint densification and nanotubes degradation is proved.

Keywords: Spark plasma sintering; Sintering; Microstructure-final; Si_3N_4; Nanotubes

1. Introduction

Among the general category of electric current activated sintering (ECAS) processes, the spark plasma sintering (SPS), which is a pressure assisted pulsed direct current sintering technique, is the most employed to consolidate powders of very different natures. Compared to conventional sintering (CS) techniques such as pressureless sintering (PS), hot pressing (HP) or hot isostatic pressing (HIP), SPS allows much faster heating rates and shorter sintering times; together with commonly lower sintering temperatures. This technique extraordinarily enhances the sinterability of most of the materials and extends the possibilities for developing new advanced materials and tailoring their properties. Until now, SPS has successfully covered a wide spectrum of materials, from metals and alloys to ceramics, including different kinds of composites and coatings, as well as graded materials. A full appraisal of ECAS methods can be seen in recent reviews by Munir et al.[1] and Orru et al.[2]

During the last 15 years, the number of papers dealing with SPS method (Fig. 1a), including papers and conference proceedings, has shown a seemingly exponential increase, reaching at present the figure of ~300 publications per year (data collected from ISI Web of Knowledge). During the first decade, the acquisition of SPS equipment and the prompt fabrication of materials to compare to well known materials processed by CS techniques was the pattern. However, current publication efforts point to the new or complex materials development as well as gaining some insight into SPS process.

On the other hand, it is well known that silicon nitride (Si_3N_4) materials present good thermo-mechanical and tribological properties, which enable them to sustain the wearing conditions enduring some engineering parts, such as valves in diesel engines, ball bearings, sealing rings or tools for metal cutting and shaping.[3] The densification of these materials commonly entails the use of α-Si_3N_4 powders plus rare earth oxides additives, and temperatures as high as 1700–1800 °C for promoting the liquid-phase sintering (LPS).[4] LPS mechanism includes particle rearrangement, solution-precipitation and Ostwald ripening grain growth stages, which usually overlap. When CS techniques (PS, HP or HIP) are employed, α → β-phase transformation and grain growth jointly occur during Si_3N_4 densification.[5] The SPS technique can enhance the sinterability of Si_3N_4 producing dense materials with controlled grain growth and phase transformation at reduced temperatures,[6–10] compared to CS processes. Since Nishimura et al.[6] reported in 1995 for the first time the densification of Si_3N_4 powders by SPS, the number of publications associated to this sintering technique on Si_3N_4-based materials (including their derivative

* Corresponding author at: Institute of Ceramics and Glass (CSIC), Campus de Cantoblanco, Kelsen, 5, 28049 Madrid, Spain. Tel.: +34 917355863; fax: +34 917355843.
E-mail address: mbelmonte@icv.csic.es (M. Belmonte).

0955-2219/$ – see front matter © 2010 Elsevier Ltd. All rights reserved.
doi:10.1016/j.jeurceramsoc.2010.01.025

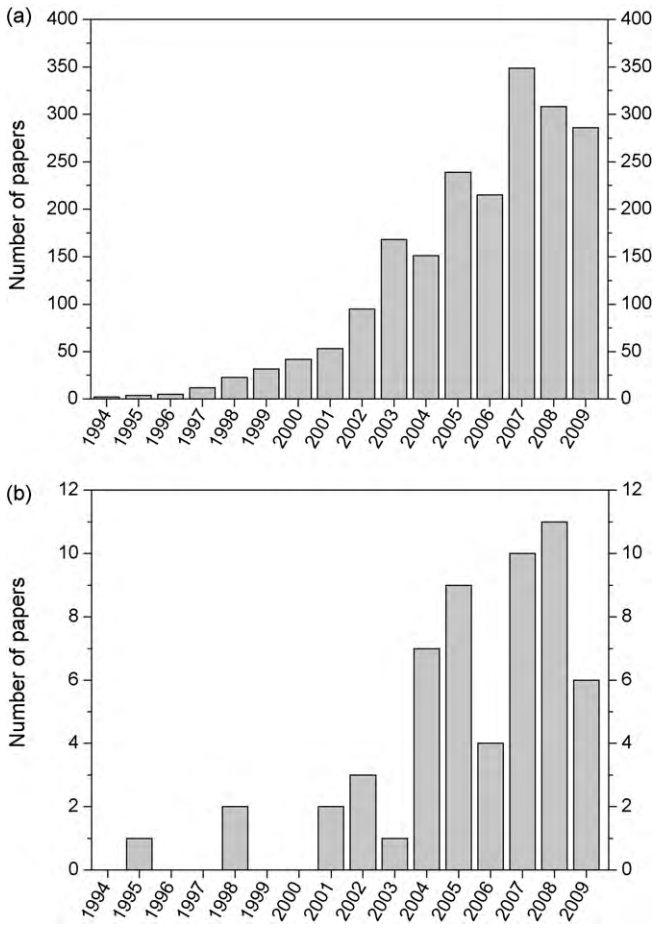

Fig. 1. Number of publications including papers and conference proceedings on: (a) SPS and (b) SPSed Si_3N_4-based materials. Numbers collected from ISI Web of Knowledge. Data for 2009 appear incomplete.

SiAlON ceramics and composites containing other ceramics or carbon-based structures)[2] has continuously increased (Fig. 1b), looking for new materials and applications.

In the present work, the potential of SPS to develop new Si_3N_4-based materials is studied in depth. First of all, we discuss the possible effect of pulsed direct current on the liquid phase formed during the sintering of Si_3N_4 ceramics. Next, we illustrate the capability of SPS for getting continuous functionally graded materials (FGMs) from a sole homogenous Si_3N_4 mixture just modifying the SPS system punches set-up in order to create a temperature gradient within the specimen. Finally, the use of SPS as the best option to attain fully dense carbon nanotubes (CNTs) containing composites avoiding the nanotubes degradation is shown.

2. SPS on Si_3N_4 ceramics

At present, the phenomena responsible for the enhanced sintering in SPS systems are still under debate.[11–21] One of the first hypothesis was the local generation of a plasma between particles when current is applied, which would cause the particle surface cleaning and then the improvement of the mass transport.[16] This hypothesis has been particularly controversial because the lack of experimental evidence of such plasma formation.[14] Among the numerous SPS mechanisms proposed, there is a general consensus on the important role of both the rapid Joule heating[17] and the intrinsic electric field effects.[15,17,18] For Sialon materials, Nygren's group[8,19,20] proposed a dynamic ripening mechanism to explain the very fast in situ formation of tough interlocking microstructures by SPS annealing dense compacts. Accordingly, the motion of charged species was enhanced by the electric field and rapid heating, which increased diffusion and homogenization in the liquid phase.[20] This mechanism may be considered as an enhanced solution-precipitation process involving a rapid grain growth. On the other hand, Salamon et al.[21] questioned the influence of electric field on α-phase formation in Sialon materials, claiming that the temperature was the main influence.

In the present work, we focus mainly on the particle rearrangement stage during the densification process of SPSed α-Si_3N_4 powders with liquid forming oxide additives. As stated above, unlike CS processes, SPS allows shortening of Si_3N_4 sintering time from hours to minutes, getting total densification with negligible grain growth and/or phase transformation.[7,8,10,22] Using a composition with 2 wt.% of Al_2O_3 and 5 wt.% of Y_2O_3 as sintering aids (SN2A5Y specimen), relatively dense ($d_{rel} > 95\%$) specimens with reduced phase transformation (76% α-phase) and negligible grain growth (190 nm) at temperatures as low as 1500 °C (Table 1) are achieved. At 1600 °C, complete dense materials that also retain high α-phase content (41%) are observed. That is, densification mainly takes place by particle rearrangement in these specimens, particularly for the low transformed specimen. However, when same composition is sintered by HP, temperatures of 1750 °C and holding times of 90 min are required to get full densification, therefore, leading to the complete α → β-phase transformation (Table 1).

Fig. 2 depicts displacement rate, d(dz)/d*t*, versus temperature during SPS of the SN2A5Y specimen. Peaks at 1280 °C and 1415 °C, linked to the particle rearrangement and the solution-precipitation sintering stages, respectively, are clearly

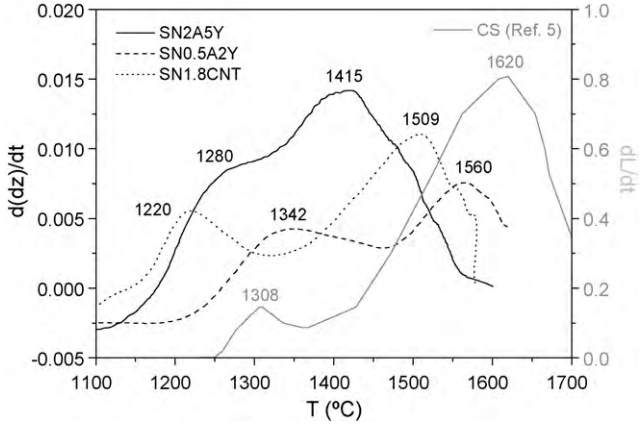

Fig. 2. Displacement rate (d(dz)/d*t*) curves versus temperature for SPSed monolithic materials with different additives contents (SN2A5Y and SN0.5A2Y compositions), and SN1.8CNT composite. Petzow's data re-plotted from Ref. [5][5] are also included.

Table 1
Sintering technique and maximum sintering temperature (T_{max}), apparent (d) and relative densities (d_{rel}), α-phase content, average particle size (d_{50}) and aspect ratio (AR_{50}), both estimated on FESEM micrographs by image analysis techniques, for SN2A5Y and SN0.5A2Y materials.

Composition	Sintering technique	T_{max} (°C)	d (g cm^{-3})	d_{rel} (%)	α-Phase (%)	d_{50} (nm)	AR_{50}
SN2A5Y		1500	3.08	95.4	76	190	1.4
	SPS	1600	3.23	100.0	41	300	1.8
		1650	3.23	100.0	6	570	2.4
	HP	1750	3.23	100.0	0		
SN0.5A2Y	SPS	1675	3.19	100.0	15		
	HP	1750	3.12	97.8	13		

SPS tests were carried out at a heating rate of 133 °C min^{-1} for 5 min of holding time, using an uniaxial pressure of 50 MPa, and a vacuum pressure of 6 Pa. HP runs were performed at heating rate of 10 °C min^{-1} for 90 min of holding time, using an uniaxial pressure of 50 MPa, under 0.1 MPa of N_2.

distinguished. Petzow and Herrmann's shrinkage rate data[5] for CSed Si_3N_4 with similar Y_2O_3/Al_2O_3 additive ratio (2.0) are re-plotted in Fig. 2 for comparison. The maximum shrinkage rate for CS occurs at higher temperature than for SPS specimens (SN2A5Y), in spite of the larger additive content of the CS specimen (6.0 vol.% versus 4.9 vol.%) and lower CS heating rate (10 °C min^{-1} versus 133 °C min^{-1}). Another interesting observation from Fig. 2 is that the intensity ratio (0.50) between both peaks, $I_{rerrangement}/I_{sol\text{-}prec}$, is twice larger for the SPSed specimen than for the CS sample (0.25). This unusual enhancement of the particle rearrangement relative to the solution-precipitation could be attributed to the existence of an electric field. Similarly as electromigration has been considered as one of the main effects in SPS of solid particles,[11,12,15] electromechanical forces acting on liquids that are in contact with a surface should be taken into account when liquids are present, such in liquid phase sintering. These forces classically act when either dielectric or aqueous liquids are in contact with a dielectric film and a voltage (ac or dc) is applied to the system. Experimentally, they manifest by a reduction of the liquid contact angle (*electowetting*) and by the *height of rise effect*,[23,24] both phenomena directly depend on the squared applied voltage, V^2, and the inverse thickness of dielectric film, d, and have been experimentally observed at room temperature in dc and ac conditions for voltages as low as 6–15 V[25,26] when d was between 20 and 70 nm. Characteristic voltages in SPS experiments are in the 4–6 V range, but considering the small particle size (200 nm) of the Si_3N_4 powders, high electric field strengths may be reached at the nano-scale contacts. As particle rearrangement shrinkage is governed by capillary forces developed in the grain boundary liquid phase, the existence electromechanical forces acting over the liquid would be a plausible explanation of the increased

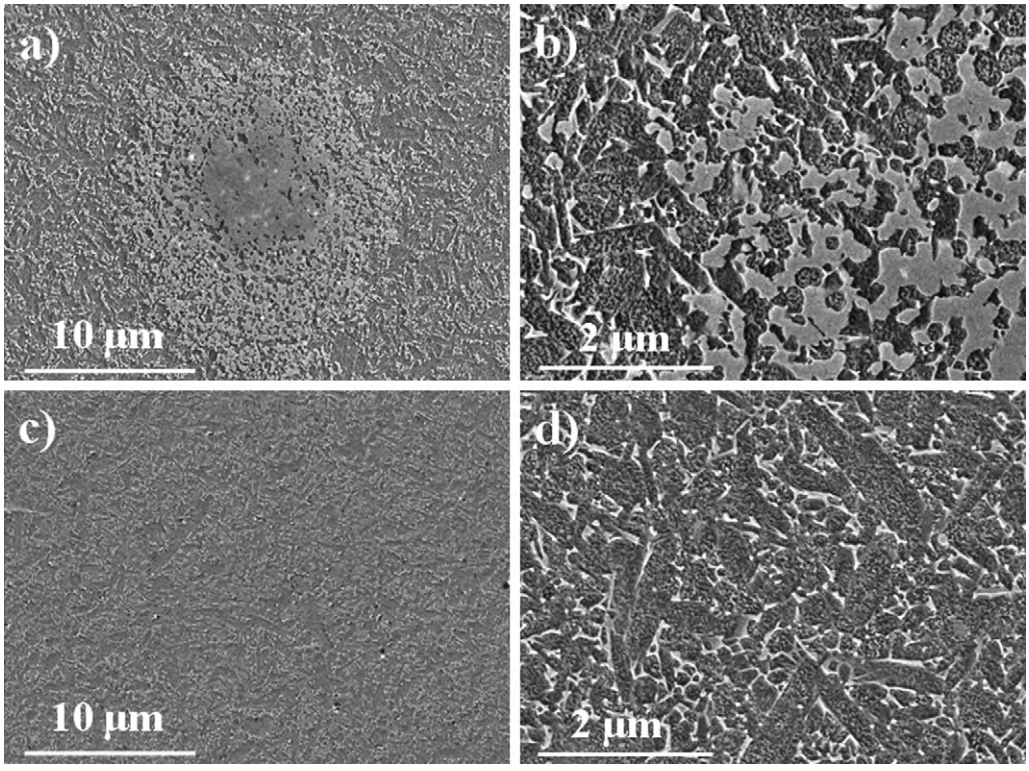

Fig. 3. FESEM micrographs of the different grain boundary glassy phase distribution attained for: (a) low and (b) high magnification HPed, and (c) low and (d) high magnification SPSed SN0.5A2Y compositions.

sintering rate generally observed during first sintering stage in SPSed Si_3N_4.

A direct experimental proof of the enhanced wetting is not an easy task as temperatures of 1400 °C, voltage application and a recording device will be necessary. Nevertheless, an indirect proof of the better wetting by the grain boundary liquid phase in SPS ceramic is obtained by comparing materials from the same powder batch, SN0.5A2Y, with a low additive content (0.5 wt.% of Al_2O_3 plus 2 wt.% of Y_2O_3), sintered alternatively by hot pressing and SPS at 1750 °C and 1600 °C, respectively. This particular composition was selected attending to its high Y_2O_3/Al_2O_3 weight ratio (∼4), thus expecting a poor liquid wettability.[27] Effectively, the HPed SN0.5A2Y specimen showed inhomogeneous distribution of the grain boundary phase with large glassy pockets like that shown in Fig. 3a and b. Conversely, the SPSed SN0.5A2Y sample has an homogeneously distributed grain boundary glassy phase like that seen in representative microstructures of Fig. 3c and d, clearly indicating the better wetting of the liquid phase if an electric field was present during sintering. Even considering the uncertainties on the real specimen temperature in SPS runs, models give a maximum difference between the surface die temperature and centre of the specimen of 150 °C, the temperature cannot be claimed as responsible of the better wetting as in the worst case specimens would have been subject to the same temperature (1750 °C) but for different time scales.

Furthermore, the solution-precipitation peak shifts ∼200 °C to lower temperatures in SPS compared to the CS. Additionally, the microstructure of SPSed SN2A5Y specimens (Fig. 4 and Table 1) rapidly evolves with temperature from sub-micron equiaxed grains with negligible grain growth (d_{50} = 190 nm and AR_{50} = 1.4) at 1500 °C, towards coarse bimodal microstructures at 1600 °C and 1650 °C (d_{50} = 300 and 570 nm, AR_{50} = 1.8 and 2.4, respectively). Grain growth during this step is linked to the corresponding α → β transformation, showing a significant decrease in the α-phase content from 76% at 1500 °C to 6% at 1650 °C (Table 1). The increased sintering rate and grain coarsening also observed in the solution-precipitation stage can be attributed to the dynamic ripening mechanism.[21]

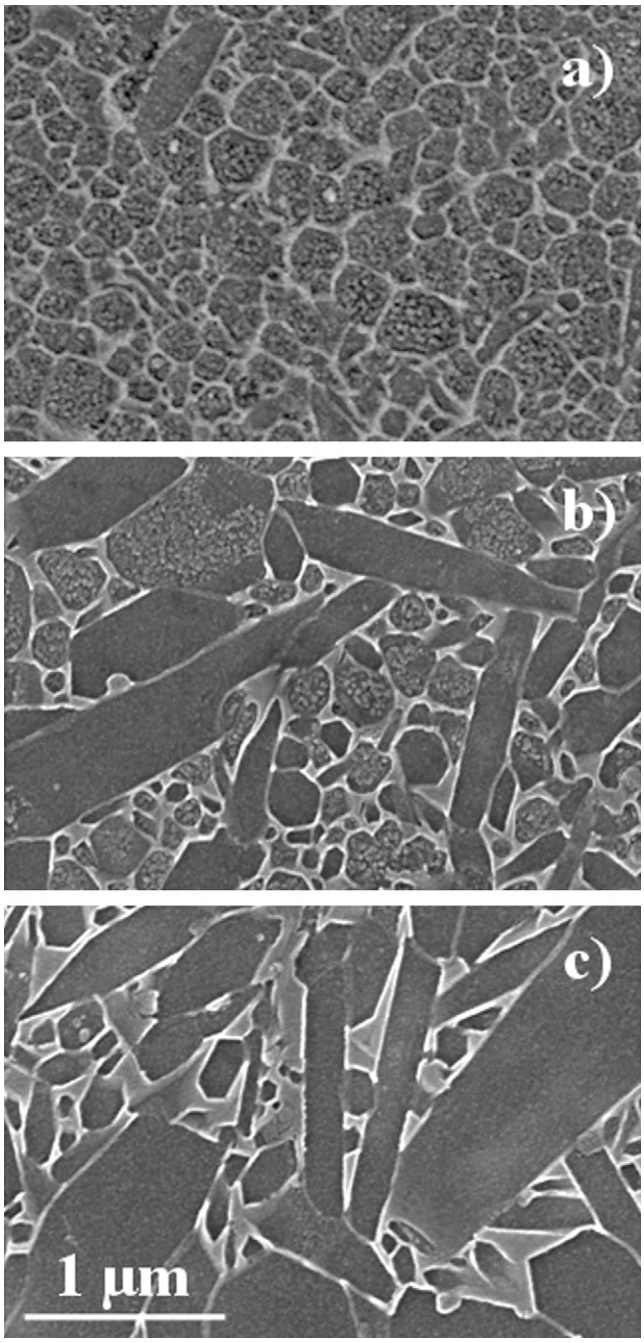

Fig. 4. FESEM micrographs of the polished and plasma etched surfaces corresponding to SPSed SN2A5Y specimens as a function of SPS temperature: (a) 1500 °C, (b) 1600 °C and (c) 1650 °C.

3. Advanced Si_3N_4 structures

The use of the SPS technique in the particular case of Si_3N_4-based ceramics offers new possibilities for tailoring microstructures. Although there are few papers[28,29] dealing with the possibility of processing continuous graded materials by SPS, this technique allows the development of temperature gradients across the compacted powders by creating a difference in the effective current intensity per unit area along the die. This can be a chance for developing unique Si_3N_4 FGMs with graded mechanical properties like high toughness and hardness values in a sole specimen, which have great technological interest.

On the other hand, SPS can have a great impact in the densification of bimodal systems like composites containing fibres or other large aspect ratio particles. During bimodal sintering internal stresses opposing densification develop due to the sintering rate differential between the 'non-densifying' inclusions and the matrix. Among ceramic composites, those containing CNTs are particularly promising but troublesome as temperature restrictions related to carbon nanotubes degradation are superimposed to constraint densification issues. These drawbacks can be overcome by SPS technique, and the possibility of getting complete densification in Si_3N_4/CNTs composites (up to 8.6 vol.%) without nanotubes degradation is described in this paper.

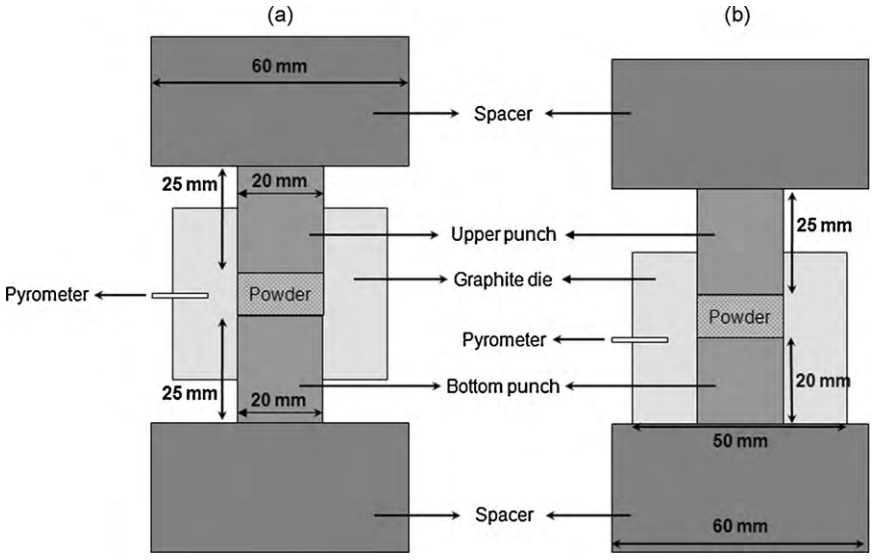

Fig. 5. (a) Symmetric and (b) asymmetric SPS configurations showing the graphite die and punches set-up.

3.1. Functionally graded Si_3N_4 materials

Materials with compositional and/or microstructural gradients, commonly known as functionally graded material (FGM), can show better performance under demanding technological applications.[30,31] Most of the published works on Si_3N_4-based FGMs consist in layered systems step-wise fabricated by stacking a number of layers with gradual variations in particle size or composition.[33–36] However, this processing method is cumbersome for mass production, and more prone to the nucleation of interfacial stresses that would compromise the reliability of the component under operating conditions. Present authors[32] processed continuous in situ functionally graded Si_3N_4 materials from a sole homogenous starting composition using an asymmetric arrangement of the SPS graphite punches to get a temperature gradient, which turned into α/β ratio[32] and, therefore, into property gradation through the Si_3N_4 specimen.

Fig. 5 compares the schemes of the SPS graphite die and punches set-up used to produce homogeneous temperature distribution with a symmetric configuration (Fig. 5a) and temperature gradients with asymmetric one (Fig. 5b). Two FGMs were fabricated at different temperatures, 1550 °C and 1650 °C. For the 1550 °C temperature set point specimen (FGM-1550) two different coloured areas were clearly observed: a dark-grey fully dense thick one and a white porous thin layer of ∼600 μm with maximum porosity of 6.5 vol.% at the bottom (Fig. 6a). Therefore, the experimental setting gave a decreasing temperature gradient within the specimen from top to bottom. For the 1650 °C (FGM-1650) the specimen, complete densification, as the homogeneous dark-grey colour along the cross-section evidenced (Fig. 6b), was attained.

A continuous α-phase gradation was confirmed by X-ray diffraction (XRD) analyses recorded every 250 μm along the cross-section from bottom to top specimen surfaces (Fig. 7). In this sense, α-content for FGM-1550 gradually changed from

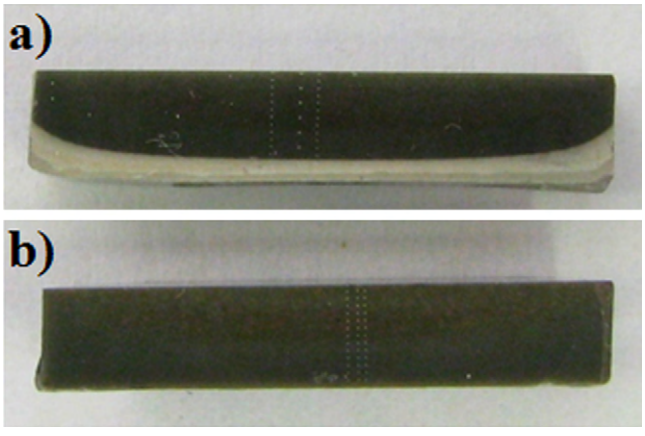

Fig. 6. Low-magnification cross-section views for: (a) FGM-1550 and (b) FGM-1650. Disc samples dimensions of 20 mm diameter and 4 mm thickness.

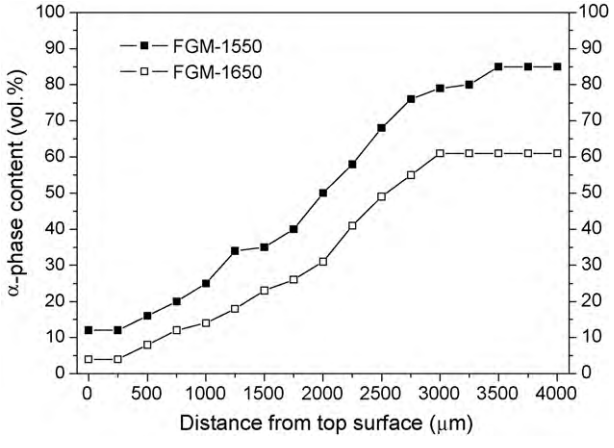

Fig. 7. α-Phase content along FGM-1550 and FGM-1650 cross-sections.

85% at the bottom to 12% at the top surface. On the other hand, for FGM-1650 specimen, α-phase content ranged from 61 to 4% (bottom to top). Comparing these percentages with those obtained using a symmetric configuration of the punches, temperature differences along the axial direction of 150 °C and 50 °C for FGM-1550 and FGM-1650, respectively, were estimated.[32]

Microstructural gradients along the specimens were confirmed by field emission scanning electron microscopy (FESEM) observations along FGM-1550 and FGM-1650 cross-sections (Fig. 8). In this way, at the bottom of FGM-1550 (Fig. 8a), the porous region presented a narrow distribution of fine equiaxed Si_3N_4 grains and, once the full dense region was reached (Fig. 8a, centre position), grain growth gradually progressed towards the top surface, leading to a bimodal microstructure of large elongated β-grains embedded into a matrix of equiaxed smaller grains. As a result, the average particle size, d_{50}, changed from 180 nm (a value similar to the original Si_3N_4 crystallite size that was ∼200 nm) to 380 nm from bottom to top, which represents an increase of ∼110%; while the average aspect ratio, AR_{50}, augmented from 1.4 to 2.3 (∼60%). At the highest temperature, FGM-1650 sample (Fig. 8b), a larger gradation in the microstructure was observed, d_{50} increasing from ∼200 to 500 nm (150%), and AR_{50} from 1.5 to 2.3 (∼50%).

These gradients, in α-phase content as well as in the microstructural parameters, determined the contour lines of hardness (H) and fracture toughness (K_{IC}) in the materials. These properties were determined by Vickers indentation methods along the cross-sections of the FGM specimens. As seen in Fig. 9a, H continuously increased up to 30% from top to bottom for both FGMs, which correlates with an augment in the harder phase content, i.e., α-phase. In the case of FGM-1550 specimen, H abruptly decreased in the porous area. On the other hand, a continuous K_{IC} gradient along the thickness of the fully dense FGM-1650 specimen (Fig. 9b), ranging from 3.5 MPa $m^{1/2}$ (bottom) to 5.7 MPa $m^{1/2}$ (top), was established, which represents more than 60% increase in K_{IC} from side

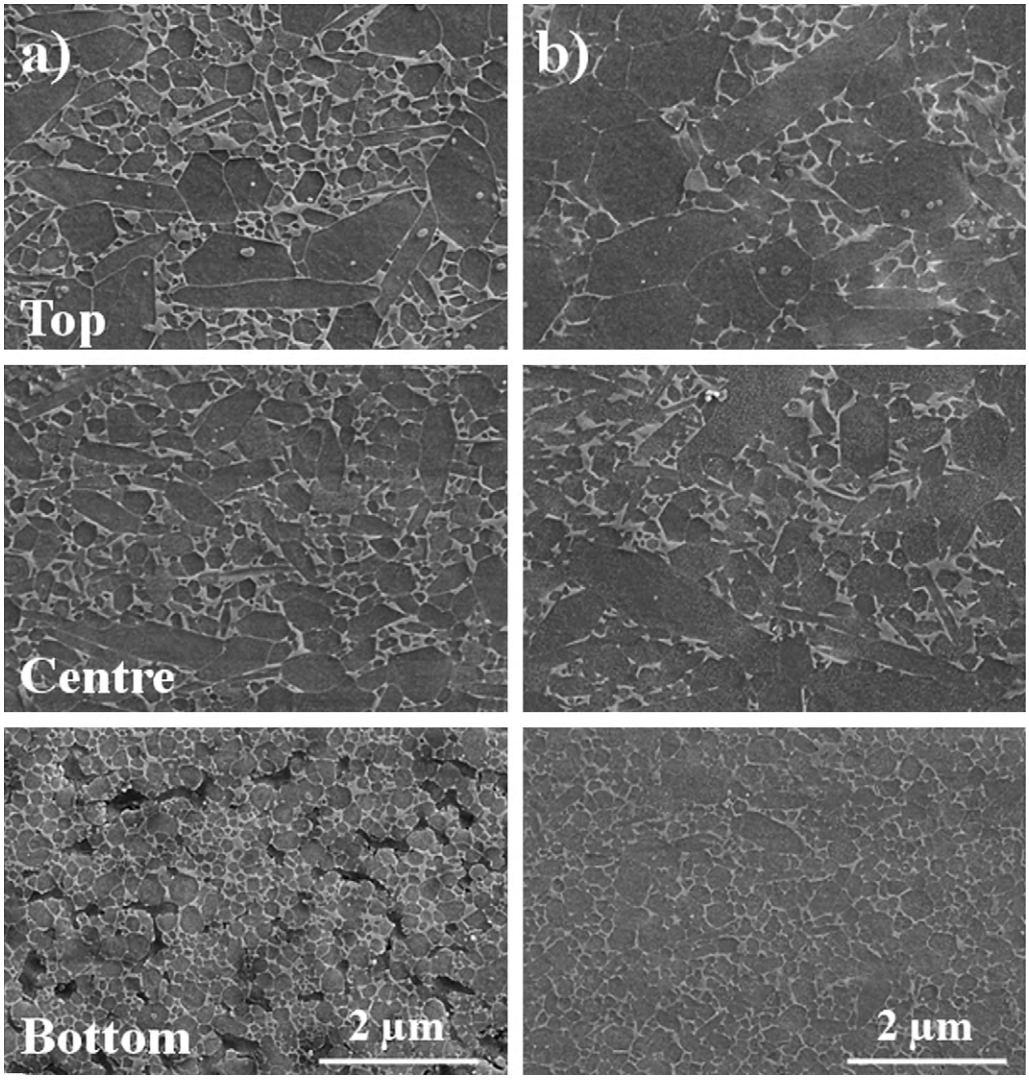

Fig. 8. FESEM micrographs of the polished and plasma etched cross-section surfaces corresponding to: (a) FGM-1550 and (b) FGM-1650, at the top, centre and bottom of each specimen.

to side. This increase is due to the development of bimodal microstructure towards top surface, then following a reverse trend to hardness.

3.2. Si_3N_4/CNTs composites

Soon after carbon nanotubes were first synthesised,[37] their extraordinary physical and mechanical properties[38,39] made them promising *fibres* for a wide range of composite materials,[39,40] especially in polymer composites and to a lesser extent in ceramic matrix composites.[41,42] Focusing on the latter, the properties reported until now are widespread and, sometimes, contradictory, especially for mechanical properties[42]; besides, they strongly depend on the type of matrix, the nanotubes kind and the processing conditions. The main efforts in the processing of ceramics/CNTs composites deal with: (i) the homogeneous dispersion of CNTs within the matrix; (ii) the complete densification of the composite avoiding nanotubes degradation; and (iii) the improvement of matrix/nanotube interface.

Although the addition of CNTs to Si_3N_4 could presumably enhance the properties of this ceramic, scarce references can be found on this topic.[43–48] Furthermore, most of the works reported insufficient CNTs dispersion, lack of density especially for large CNTs contents, and/or nanotubes degradation, the last two problems being associated to the use of conventional sintering techniques. The first problem is due to the difficulty in getting homogenous dispersions of Si_3N_4 powders, the sintering additives and the CNTs. Osendi et al.[48] obtained quite homogenous Si_3N_4/CNTs composites with up to 5.3 vol.% of multi-walled carbon nanotubes (MWCNTs) by separately dispersing the ceramic slurry and the MWCNTs and, afterwards, mixing both suspensions in ethanol combining sonication and mechanical stirring procedures.

Full densification of these composites is another challenge due to the high temperatures and long times usually required for sintering Si_3N_4 materials when CS techniques are employed, which bring doubts about the possible degradation of nanotubes throughout the sintering process. In this context, SPS with their fast heating rates and lower temperatures appears as the unique technique to overcome this problem. At present, just few attempts to sinter Si_3N_4/CNTs composites using SPS have been reported[44,46,48] and more studies are needed. Next, the quite promising results obtained by the present authors are summarized.

Following the procedure detailed in a previous paper,[48] composites containing 1.8, 5.3 and 8.6 vol.% of MWCNTs, labelled as SN1.8CNT, SN5.3CNT and SN8.6CNT, respectively, were fabricated by SPS. The addition of the highly electrical conductive CNT second phase to Si_3N_4 modified the shrinkage behaviour during SPS of composites compared to electrical insulator monolithic Si_3N_4 (Fig. 2). Just by introducing 1.8 vol.% of MWCNTs the peak temperature linked to the particle rearrangement stage of SN2A5Y composition decreased ~60 °C. The changes in the dc electrical conductivity in Si_3N_4 ceramics from electrical insulator to semiconductor with small MWCNTs additions[45,49] would modify the SPS

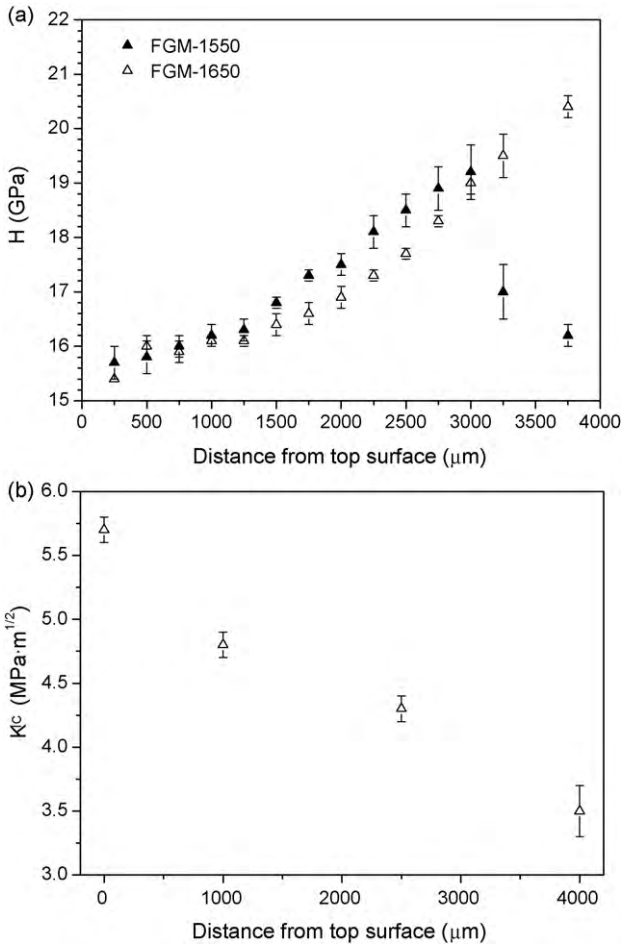

Fig. 9. (a) Hardness (H) along the cross-section of the FGM-1550 and FGM-1650 specimens and (b) fracture toughness (K_{IC}) along the dense FGM-1650 specimen. H and K_{IC} were determined by Vickers indentation methods using loads of 49 and 490 N, respectively.

behaviour, affecting not only the specimens Joule heating but also the liquid wetting as nanotubes may now act as local electrodes, then explaining the shift of the particle rearrangement peak to lower temperatures. Besides, the temperature of the solution-precipitation peak for the composite is ~100 °C higher than for the monolithic material (Fig. 2), probably because the MWCNTs network envelops Si_3N_4 grains hindering further densification.[50,51] The $I_{rerrangement}/I_{sol\text{-}prec}$ ratio for all the composites was around 0.50, which is similar to the value for the SPSed monolithic material of same composition (Fig. 2).

SPS allowed attaining complete densification for all the composites, avoiding at the same time nanotubes degradation as micro-Raman spectroscopy data confirmed (Fig. 10). In fact, the intensity ratios between the characteristics bands of MWCNTs, i.e., D/G and G′/G,[52] were quite similar in the composites and original nanotubes. As the plasma etching procedure used for revealing polished surface microstructures in Si_3N_4 (CF_4/5 vol.% O_2 at 100 W for 40 s) damages the MWCNTs (Fig. 11a), these are better detected on fresh fracture surfaces where the outcropping of CNTs is evident (Fig. 11b–d). In this figure, the good dispersion of MWCNTs is plain, even for rel-

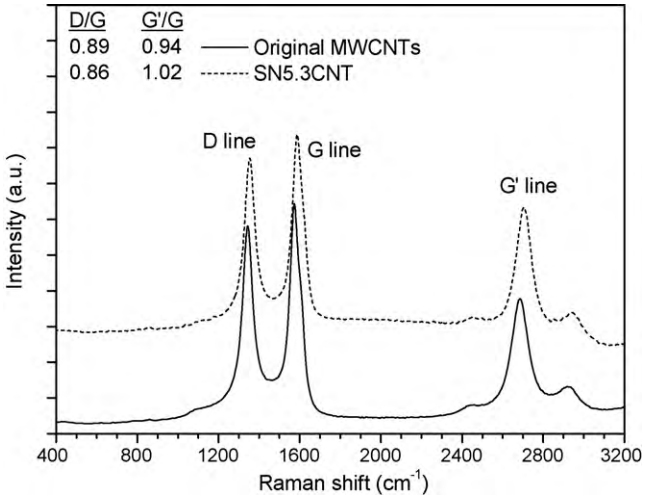

Fig. 10. Micro-Raman spectra for the original MWCNTs and SN5.3CNT composite. D/G and G′/G intensity ratios are depicted on top left corner.

atively high nanotubes contents (up to 8.6 vol.%, Fig. 11d). Transmission electron microscopy (TEM) observations confirmed that MWCNTs were bent and twisted at Si_3N_4 grain boundaries (Fig. 12).

The comparison of microstructural parameters, d_{50} and AR_{50}, between the monolithic and the composites with similar α-phase contents (~40%), revealed a Si_3N_4 grain size refinement attributable to the MWCNTs (Table 2), which can be quantify as 22% and 13% for d_{50} and AR_{50}, respectively, due to the hindering of the solution-precipitation stage by the bimodal sintering.

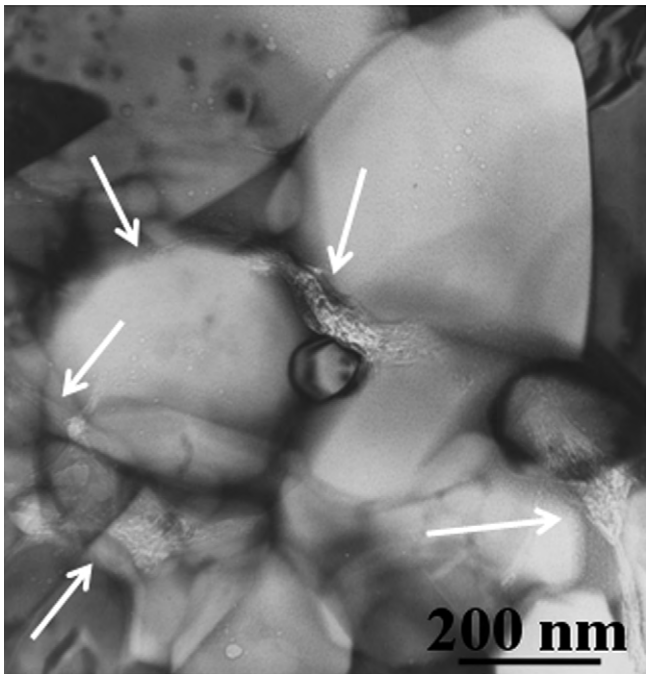

Fig. 12. TEM micrograph for the SN5.3CNT composite. The nanotubes are pointed out by arrows.

Controversial results can be found in the literature regarding the supposed reinforcement capability of CNTs in ceramic composites.[42,53,54] As an example, for Al_2O_3/10 vol.% single-walled carbon nanotubes (SWCNTs),[53,54] disparate toughness values, 3.3[54] and 9.7[53] MPa $m^{1/2}$, were reported. For present

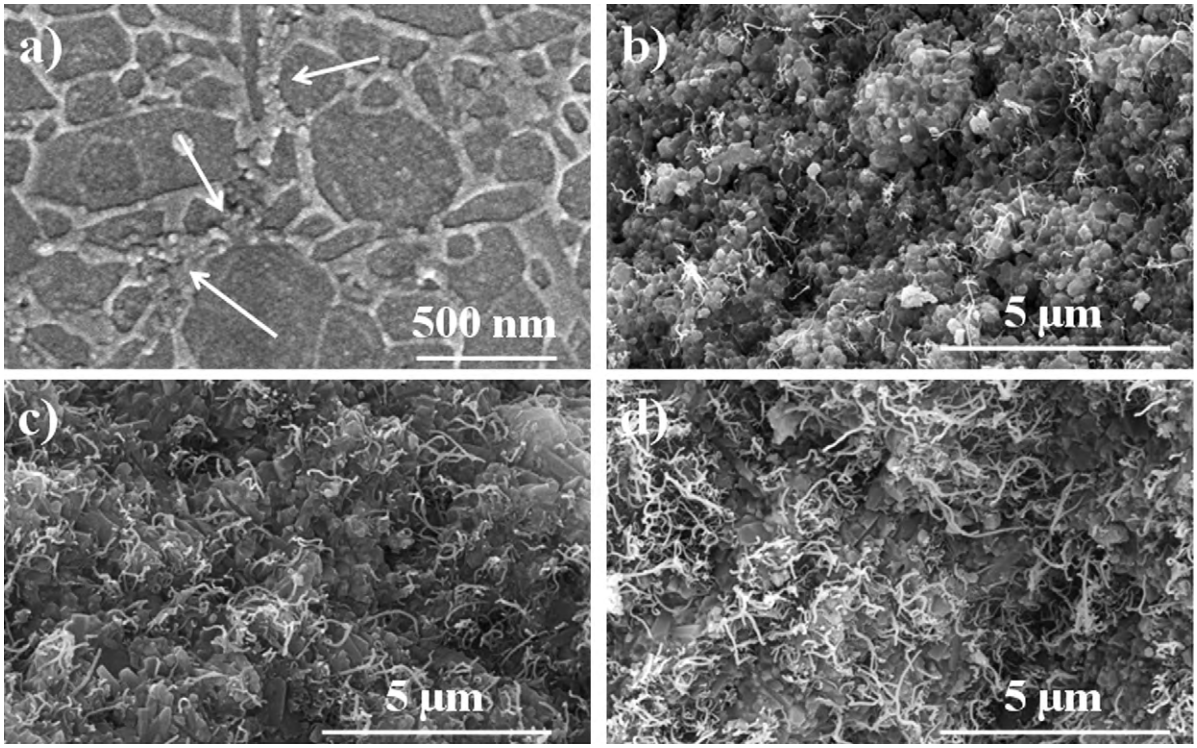

Fig. 11. FESEM micrographs showing polished and plasma etched surface of SN8.6CNT composite (a) and fracture surfaces of Si_3N_4/MWCNTs composites containing: (b) 1.8 vol.%, (c) 5.3 vol.% and (d) 8.6 vol.% of MWCNTs. Arrows in (a) point nanotubes.

Table 2
α-Phase content, average particle size (d_{50}), aspect ratio (AR_{50}), and electrical conductivity (σ) for Si_3N_4/MWCNTs composites.

Sample ID	α-Phase (%)	d_{50} (nm)	AR_{50}	σ (S m^{-1})
SN2A5Y	41	297	1.79	3×10^{-13}
SN1.8CNT	41	245	1.67	3×10^{-1}
SN5.3CNT	34	237	1.51	14
SN8.6CNT	43	233	1.56	17

d_{50} and AR_{50} were estimated on FESEM micrographs by image analysis techniques. Either two of four probe methods under dc conditions were used to measure σ.

materials,[48] K_{IC} data, determined by Vickers indentation at 196 N, slightly increased from 4.5 MPa m$^{1/2}$ for the monolithic material to 4.8 MPa m$^{1/2}$ in the SN1.8CNT composite. However, for larger MWCNTs contents (5.3 vol.%), K_{IC} decreased to 4.2 MPa m$^{1/2}$, which could be associated to a poorly bonded matrix/nanotube interface. Published data for Si_3N_4/CNTs composites report either negligible changes in K_{IC}[44,45] or large increases.[46,47] Corral et al.[46] reported an increase in K_{IC} from 5.3 to 8.5 MPa m$^{1/2}$ just by adding 2 vol.% of SWCNTs, although the composite presented larger porosity than the monolithic and microstructural data were not provided. Pasupuleti et al.[47] also reported an increase in K_{IC} from 4.8 to 6.6 MPa m$^{1/2}$ with 1 wt.% of MWCNTs, but this increase may be as well due to the greater fraction of elongated Si_3N_4 grains in the composite producing the well known in situ toughening. It is important to remark that the mechanical properties of Si_3N_4 ceramics are very sensitive to microstructure (porosity, α/β ratio, grain size and aspect ratio distributions), and therefore it is very difficult to determine the real toughening effect of CNTs if dissimilar microstructures are compared.

Conversely, much agreement is found when comparing the electrical conductivity data for Si_3N_4/CNTs composites. As seen in Table 2, the dc electrical conductivity of the present Si_3N_4/MWCNTs composites showed a raise of twelve orders of magnitude for SN1.8CNT specimen compared to the monolithic material, reaching a saturation value of 17 S m^{-1} for the material with the largest nanotubes content (SN8.6CNT). These results are similar to those reported by Tatami et al.[45] The turning of Si_3N_4 ceramics from highly electric insulator to conductor at very low CNTs concentrations, instead of the larger amounts (30–40 vol.%) needed in the case of other electric conductive second phases, such as TiN,[55] can have exciting technological applications such as the electric discharge machining (EDM) of Si_3N_4 components, which could reduce the machining costs during manufacturing processes.

In summary, SPS technique is currently a powerful research tool for developing new materials. However, the complete understanding of the phenomena that take place during the sintering process is one step behind and new models including the electric filed effects are needed. The SPS technique has strong potential for designing Si_3N_4 materials with tailored microstructures and properties. Besides, it appears as the best tool to achieve full densification of new ceramic composites containing graphite structures (CNTs, graphene) avoiding their degradation.

Acknowledgements

The financial support of Spanish Ministry of Science and Innovation through projects MAT2006-7118 and HA2007-0083 is recognized. J. Gonzalez-Julian acknowledges the financial support of the JAE (CSIC) fellowship Program.

References

1. Munir ZA, Anselmi-Tamburini U, Ohyanagi M. The effect of electric field and pressure on the synthesis and consolidation of materials: a review of the spark plasma sintering method. *J Mater Sci* 2006;**41**:763–77.
2. Orru R, Licheri R, Locci AM, Cincotti A, Cao G. Consolidation/synthesis of materials by electric current activated/assisted sintering. *Mater Sci Eng R* 2009;**63**:127–287.
3. Riley FL. Silicon nitride and related materials. *J Am Ceram Soc* 2000;**83**:245–65.
4. Suttor D, Fischman GS. Densification and sintering kinetics in sintered silicon nitride. *J Am Ceram Soc* 1992;**75**:1063–7.
5. Petzow G, Herrmann M. Silicon nitride ceramics. *Struct Bond* 2002;**102**:47–167.
6. Nishimura T, Mitomo M, Hirotsuru H, Kawahara M. Fabrication of silicon-nitride nano-ceramics by spark plasma sintering. *J Mater Sci Lett* 1995;**14**:1046–7.
7. Suganuma M, Kitagawa Y, Wada S, Murayama N. Pulsed electric current sintering of silicon nitride. *J Am Ceram Soc* 2003;**86**:387–94.
8. Shen Z, Peng H, Liu J, Nygren M. Conversion from nano- to micron-sized structures: experimental observations. *J Eur Ceram Soc* 2004;**24**:3447–52.
9. Xu X, Nishimura T, Hirosaki N, Xie RJ, Zhu Y, Yamamoto Y, et al. New strategies for preparing nanosized silicon nitride ceramics. *J Am Ceram Soc* 2005;**88**:934–7.
10. Peng GH, Liang M, Liang ZH, Li QY, Li WL, Liu Q. Spark plasma sintering silicon nitride ceramics with high thermal conductivity using $MgSiN_2$ as additives. *J Am Ceram Soc* 2009;**92**:2122–4.
11. Bertolino N, Garay J, Anselmi-Tamburini U, Munir ZA. Electromigration effects in Al–Au multilayers. *Scripta Mater* 2001;**44**:737–42.
12. Olevsky EA, Kandukuri S, Froyen L. Consolidation enhancement in spark-plasma sintering: impact of high heating rates. *J Appl Phys* 2007;**102**:114913.
13. Chaim R. Densification mechanisms in spark plasma sintering of nanocrystalline ceramics. *Mater Sci Eng A* 2007;**443**:25–32.
14. Hulbert DM, Anders A, Dudina DV, Andersson J, Jiang D, Unuvar C, et al. The absence of plasma in spark plasma sintering. *J Appl Phys* 2008;**104**:033305.
15. Olevsky EA, Froyen L. Impact of thermal diffusion on densification during SPS. *J Am Ceram Soc* 2009;**92**:S122–32.
16. Groza JR, Garcia M, Schneider JA. Surface effects in field-assisted sintering. *J Mater Res* 2001;**16**:286–92.
17. Anselmi-Tamburini U, Gennari S, Garay JE, Munir ZA. Fundamental investigations on the spark plasma sintering/synthesis process. II. Modelling of current and temperature distributions. *Mater Sci Eng A* 2005;**394**:139–48.
18. Tokita M. Mechanism of spark plasma sintering and its application to ceramics. *Nyu Seramikkusu* 1997;**10**:43–53.
19. Shen Z, Nygren M. Kinetic aspects of superfast consolidation of silicon nitride based ceramics by spark plasma sintering. *J Mater Chem* 2001;**11**:204–7.
20. Shen ZJ, Zhao Z, Peng H, Nygren M. Formation of tough interlocking microstructures in silicon nitride ceramics by dynamic ripening. *Nature* 2002;**417**:266–9.
21. Salamon D, Shen Z, Sajgalik P. Rapid formation of α-Sialon during spark plasma sintering: its origin and implications. *J Eur Ceram Soc* 2007;**27**:2541–7.
22. Belmonte M, de Pablos A, Miranzo P, Osendi MI. Spark plasma sintering of Si_3N_4-based materials. In: Grin Y, Kieback B, Schmidt J, editors. *Pro-*

ceedings of advanced processing for novel functional materials. Dresden: Max–Plank-Institut für Chemische Physik fester Stoffe; 2009. pp. 41–46.
23. Mugele F, Baret JC. Electrowetting: from basics to applications. *J Phys Condens Matter* 2005;**17**:R705–74.
24. Jones TB, Wang KL, Yao DJ. Frequency-dependent electromechanics of aqueous liquids: electrowetting and dielectrophoresis. *Langmuir* 2004;**20**:2813–8.
25. Moon H, Cho SK, Garrell RL, Kim CJ. Low voltage electrowetting-on-dielectric. *J Appl Phys* 2002;**92**:4080–7.
26. Li Y, Parkes W, Haworth LI, Ross AWS, Stevenson JTM, Walton AJ. Room-temperature fabrication of anodic tantalum pentoxide for low-voltage electrowetting on dielectric (EWOD). *J Microelectromech Syst* 2008;**17**:1481–8.
27. Lemercier H, Rouxel T, Fargeot D, Besson JL, Piriou B. Yttrium SiAlON glasses: structure and mechanical properties—elasticity and viscosity. *J Non-Cryst Solids* 1996;**201**:128–45.
28. Japanese patent, number JP2006118033. Method for producing compositionally gradient cemented carbides.
29. Hulbert DM, Jiang D, Anselmi-Tamburini U, Unuvar C, Mukherjee AK. Experiments and modeling of spark plasma sintered, functionally graded boron carbide–aluminum composites. *Mater Sci Eng A* 2008;**488**:333–8.
30. Hirai T. In: Brook RJ, editor. *Materials science and technology—a comprehensive treatment*, vol. 17B, Part 2. Weinheim, Germany: Wiley–VCH; 1996. p. 293.
31. Neubrand A, Rödel J. Gradient materials: an overview of a novel concept. *Z Metallkd* 1997;**88**:358–71.
32. Belmonte M, Gonzalez-Julian J, Miranzo P, Osendi MI. Continuous in situ functionally graded silicon nitride materials. *Acta Mater* 2009;**57**:2607–12.
33. Jiang X, Baek YK, Lee SM, Kang SJL. Formation of an α-SiAlON layer and its effect on mechanical properties. *J Am Ceram Soc* 1998;**81**:1907–12.
34. Lee KS, Lee SK, Lawn BR, Kim DK. Contact damage and strength degradation in brittle/quasi-plastic silicon nitride bilayers. *J Am Ceram Soc* 1998;**81**:2394–404.
35. Pender DC, Padture NP, Giannakopoulos AE, Suresh S. Gradients in elastic modulus for improved contact-damage resistance. Part I. The silicon nitride-oxynitride glass system. *Acta Mater* 2001;**49**:3255–62.
36. Acikbas NC, Suvaci E, Mandal H. Fabrication of functionally graded SiAlON ceramics by tape casting. *J Am Ceram Soc* 2006;**89**:3255–7.
37. Iijima S. Helical microtubules of graphitic carbon. *Nature* 1991;**354**: 56–8.
38. Popov VN. Carbon nanotubes: properties and application. *Mater Sci Eng R* 2004;**43**:61–102.
39. Harris PJF. *Carbon nanotube science. Synthesis, properties and applications*. Cambridge, England: Cambridge University Press; 2009.
40. Harris PJF. Carbon nanotube composites. *Int Mater Rev* 2004;**49**: 31–43.
41. Peigney A, Laurent C. In: Low IM, editor. *Ceramic matrix composites: microstructure–property relationship*. Cambridge, England: Woodhead Publishing Limited; 2006. p. 309.
42. Cho J, Boccaccini AR, Shaffer MSP. Ceramic matrix composites containing carbon nanotubes. *J Mater Sci* 2009;**44**:1934–51.
43. Balazsi Cs, Kónya Z, Wéber F, Biró LP, Arató P. Preparation and characterization of carbon nanotube reinforced silicon nitride composites. *Mater Sci Eng C* 2003;**23**:1133–7.
44. Balazsi Cs, Shen Z, Kónya Z, Kasztovszky Zs, Wéber F, Vértesy Z, et al. Processing of carbon nanotube reinforced silicon nitride composites by spark plasma sintering. *Compos Sci Technol* 2005;**65**:727–33.
45. Tatami J, Katashima T, Komeya K, Meguro T, Wakihara T. Electrically conductive CNT-dispersed silicon nitride ceramics. *J Am Ceram Soc* 2005;**88**:2889–93.
46. Corral EL, Cesarano III J, Shyam A, Lara-Curzio E, Bell N, Stuecker J, et al. Engineered nanostructures for multifunctional single-walled carbon nanotube reinforced silicon nitride nanocomposites. *J Am Ceram Soc* 2009;**91**:3129–37.
47. Pasupuleti S, Peddetti R, Santhanama S, Jena K-P, Wing ZN, Hecht M, et al. Toughening behavior in a carbon nanotube reinforced silicon nitride composite. *Mater Sci Eng A* 2008;**491**:224–9.
48. Osendi MI, Gautheron F, Miranzo P, Belmonte M. Dense and homogenous silicon nitride composites containing carbon nanotubes. *J Nanosci Nanotechnol* 2009;**9**:6188–94.
49. Gonzalez-Julian, J., Iglesias, Y., Caballero, A. C., Belmonte, M., Garzon, L., Ocal, C., Miranzo, P., Osendi, M. I., Multi-scale electrical response of silicon nitride/multi-walled carbon nanotubes composites. Acta Mater, submitted for publication.
50. Sudre O, Bao G, Fan B, Lange FF, Evans AG. Effect of inclusions on densification. II. Numerical model. *J Am Ceram Soc* 1992;**75**:525–31.
51. Belmonte M, Moya JS, Miranzo P. Bimodal sintering of Al_2O_3/Al_2O_3 platelet ceramic composites. *J Am Ceram Soc* 1995;**78**:1661–7.
52. DiLeo RA, Landi BJ, Raffaelle RP. Purity assessment of multiwalled carbon nanotubes by Raman spectroscopy. *J Appl Phys* 2007;**101**:064307.
53. Zhan GD, Kuntz JD, Wan JL, Mukherjee AK. Single-wall carbon nanotubes as attractive toughening agents in alumina-based nanocomposites. *Nat Mater* 2003;**2**:38–42.
54. Wang X, Padture NP, Tanaka H. Contact-damage-resistant ceramic/single-wall carbon nanotubes and ceramic/graphite composites. *Nat Mater* 2004;**3**:539–44.
55. Liu CC, Huang JL. Effect of the electrical discharge machining on strength and reliability of TiN/Si_3N_4 composites. *Ceram Int* 2003;**29**:679–87.